J. Fluid Mech. (1990), *vol.* 221, *pp.* 53–76
Printed in Great Britain

A theoretical study of two-phase flow through a narrow gap with a moving contact line: viscous fingering in a Hele-Shaw cell

By STEVEN J. WEINSTEIN,[1] E. B. DUSSAN V.[2] AND LYLE H. UNGAR[3]

[1] Emulsion Coating Technologies, Building 35, 2nd Floor, Eastman Kodak Company, Rochester, NY 14652-3701, USA

[2] Schlumberger-Doll Research, Old Quarry Road, Ridgefield, CT 06877, USA

[3] University of Pennsylvania, Department of Chemical Engineering, 220 S. 33rd Street, Towne Building, Philadelphia, PA 19104, USA

(Received 5 June 1989)

The problem of viscous fingering in a Hele-Shaw cell with moving contact lines is considered. In contrast to the usual situation where the displaced fluid coats the solid surface in the form of thin films, here, both the displacing and the displaced fluids make direct contact with the solid. The principal differences between these two situations are in the ranges of attainable values of the gapwise component of the interfacial curvature (the component due to the bending of the fluid interface across the small gap of the Hele-Shaw cell), and in the introduction of two additional parameters for the case with moving contact lines. These parameters are the receding contact angle, and the sensivity of the dynamic angle to the speed of the contact line. Our objective is the prediction of the shape and widths of the fingers in the limit of small capillary number, $U\mu/\sigma$. Here, U denotes the finger speed, μ denotes the dynamic viscosity of the more viscous displaced fluid, and σ denotes the surface tension of the fluid interface. As might be expected, there are similarities and differences between the two problems. Despite the fact that different equations arise, we find that they can be analysed using the techniques introduced by McLean & Saffman and Vanden-Broeck for the thin-film case. The nature of the multiplicity of solutions also appears to be similar for the two problems. Our results indicate that when contact lines are present, the finger shapes are sensitive to the value of the contact angle only in the vicinity of its nose, reminiscent of experiments where bubbles or wires are placed at the nose of viscous fingers when thin films are present. On the other hand, in the present problem at least two distinct velocity scales emerge with well-defined asymptotic limits, each of these two cases being distinguished by the relative importance played by the two components of the curvature of the fluid interface. It is found that the widths of fingers can be significantly smaller than half the width of the cell.

1. Introduction

The principal objective of this work is to provide a better understanding of immiscible fluid displacement at relatively slow speeds through a narrow gap formed between two solid surfaces. The essential characteristic is the small size of the gap, b, compared to the extent of the surfaces, $2W$, which allows a simplification of the

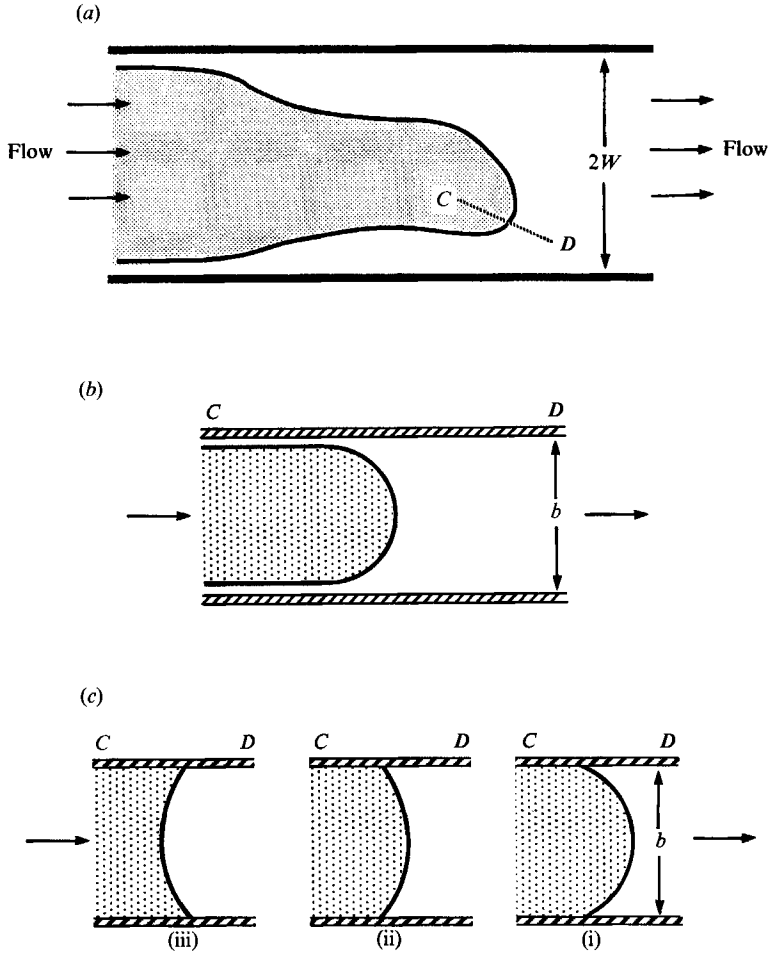

FIGURE 1. Fluid A (shaded area) displacing fluid B (unshaded area) from a gap formed between two rectangular solid plates. (*a*) Plan view. (*b*) Side view along CD direction for the case where only fluid B contacts the solid. (*c*) Side view along CD direction for the case when both fluids A and B contact the solid, where (i), (ii), and (iii) denote three possible configurations of the fluid interface.

equations and boundary conditions governing the dynamics of immiscible fluids. The use of the ratio of lengthscales in this manner is by no means new. There have been numerous studies over the past thirty years with the same objective, a substantial portion of these concerned with the problem of a less viscous fluid displacing a more viscous immiscible fluid in a Hele-Shaw cell. However, almost all have been restricted to materials in which only the more viscous fluid makes contact with the solid surfaces.

Figure 1 illustrates the central difference between the two situations where only one fluid and both fluids contact the solid surface. Here, fluid A is displacing fluid B through a gap formed between two parallel solid surfaces, where $b/W \ll 1$, i.e. a Hele-Shaw cell (refer to figure 1*a*). A cross-sectional view along the cut C–D for the two configurations of concern is given in figure 1(*b*) and 1(*c*). When only one fluid contacts the surface (figure 1*b*), in this case fluid B, at least a film of this fluid must be present on the entire solid surface; its thickness depends on the speed at which the fluid interface moves through the cell (Bretherton 1961; Tabeling, Zocchi &

Libchaber 1987; Reinelt & Saffman 1985; Reinelt 1987*a*). For this case, the fluid interface always appears to be bellowing into the fluid being displaced. Under conditions of small capillary number, $U\mu/\sigma$, i.e. values less than say 0.01, the shape of the fluid interface from this perspective is approximately that of an arc of a circle with radius slightly *smaller* than $\frac{1}{2}b$. Here, μ denotes the viscosity of fluid B, σ denotes the surface tension of the fluid interface, and U denotes the characteristic speed of the interface. However, when a moving contact line is present under similar conditions, the radius of the almost circular fluid interface may vary between $-\infty$ and $-\frac{1}{2}b$, or, $\frac{1}{2}b$ and ∞, the negative values reflecting the fact that the fluid interface may bellow into fluid A even though fluid B is being displaced (refer to figure 1*c*).

One might anticipate that the situation depicted in figure 1(*c*) would be more difficult to analyse than that depicted in figure 1(*b*), owing to the presence of moving contact lines. When moving contact lines are present, the hydrodynamic model of the fluids is not completely known (refer to Dussan V. 1979 for more details). The situation in figure 1(*b*) is free of this difficulty. However, by restricting our attention to relatively small capillary numbers, thus enabling us to take advantage of the progress made over the last decade in modelling moving contact line problems. It turns out that the resulting boundary-value problem with moving contact lines is rather straightforward to analyse. Demonstrating this point is one of the objectives of this study. This will be accomplished by examining the dynamics of a viscous finger moving through a Hele-Shaw cell.

Saffman & Taylor (1958) were the first to study the steady viscous fingering problem in a Hele-Shaw cell. Our attention is restricted to the case of a viscous liquid being displaced by a finger of gas in a horizontal cell. Saffman & Taylor used a small aspect ratio, b/W, to greatly simplify the governing equation and boundary conditions. For the governing equations, they assumed

$$\boldsymbol{u} = -\frac{b^2}{12\mu}\boldsymbol{\nabla} p, \tag{1.1}$$

$$\boldsymbol{\nabla}\cdot\boldsymbol{u} = 0, \tag{1.2}$$

where $\boldsymbol{u}$ denotes the velocity averaged across the gap, and p denotes the pressure. The conditions at the boundary of the finger, i.e. the fluid interface, were assumed to be

$$\boldsymbol{u}\cdot\hat{\boldsymbol{n}} = 0, \tag{1.3}$$

$$p = -\sigma\frac{2}{b}, \tag{1.4}$$

where $\hat{\boldsymbol{n}}$ denotes the unit normal to the line representing the location of the boundary of the finger in this two-dimensional description of the system. The first expression assumes that the gas completely expels the liquid, even though thin films were always present in the solid surfaces in their experiments. The second expression is a consequence of assuming that the pressure of the liquid at the interface obeys the same condition as under static conditions. This implies that the pressure equals $\sigma(1/R_1+1/R_2)$, where R_1 and R_2 denote the principal radii of curvature of the interface; here, R_1 is associated with the gapwise component of the interfacial curvature, while R_2 is primarily associated with the curvature of the line representing the location of the boundary of the finger, i.e. the spanwise component of the interfacial curvature. For a small aspect ratio, Saffman & Taylor approximated $1/R_1$ with $2/b$, and further assumed $1/R_2 \ll 2/b$. Using these equations and boundary

conditions, Saffman & Taylor were able to obtain an analytic expression for the shape of the finger, parametrized in terms of its upstream width, $2\lambda W$. However, no expression appeared from which λ could be determined. Experimentally, they measured the shape of a finger moving in the cell over a range of speeds. They found that the finger width varied inversely with speed, asymptoting to a value of $\frac{1}{2}W$ at fast speeds, to within their experimental error. They also found that the shape of the finger predicted by their theory agrees very well with their experimental measurements when λ equals $\frac{1}{2}$; however, the larger the value of $\lambda - \frac{1}{2}$, the greater the discrepancy between experiment and theory. Since this discrepancy is characterized by the theoretically determined finger having too broad a nose, they speculated that the pressure, instead of being constant, must increase along the interface moving away from the nose. They further speculated that the variation in pressure along the finger could only be attributed to surface tension. They cited as possible causes a varying non-zero contact angle, a non-negligible contribution from $1/R_2$, or a 'dynamic' surface-tension effect (the surface tension of a newly formed surface may change as the surface ages). However, they were unable to provide a physical explanation for $\lambda \to \frac{1}{2}$ at fast finger speeds.

The problem was reconsidered in 1981 by McLean & Saffman. They modified the boundary-value problem of Saffman & Taylor by including the term σ/R_2 in the pressure boundary condition, which resolved many of the issues (although, as pointed out by Park & Homsey (1984), they neglected a higher-order correction to $1/R_1$). They found excellent agreement between their predicted and the experimentally measured finger shapes only if the value of λ was chosen to match that of the experiment. Their analysis also determined a dependence of λ on a dimensionless finger speed, $(\mu U/\sigma)\, W^2/b^2$, with the property that $\lambda \to \frac{1}{2}$ for large finger speeds. However, the theory significantly under predicted λ, for a given value of $(\mu U/\sigma)\, W^2/b^2$, when compared with experimental data, that is to say, 'significant' when considering the degree of agreement between theory and experiment in the finger shapes. Romero (1981) showed that the solution of McLean & Saffman is not unique by finding two additional sets of finger shapes over a range of finger speeds. He further investigated the effect of incorporating a variation in the gapwise curvature, $2/b$, of the form cU_n, where c is a constant and U_n denotes the local speed of propagation of the finger as viewed from a frame of reference at rest with respect to the solid surfaces. However, Romero found that it was necessary to include σ/R in order to get isolated sets of solutions. When he set σ/R equal to zero while retaining cU_n, he obtained a continuous spectrum of solutions, a situation similar to that encountered by Saffman & Taylor. Vanden-Broeck (1983) provided evidence that the three isolated sets of solutions thus far identified are members of a denumerable infinite set. Work by Kessler & Levine (1985) and Bensimon (1986) indicated that the solution identified by McLean & Saffman is in fact the only stable solution, at least for modest values of $(\mu U/\sigma)\, W^2/b^2$. This was further supported by Tanveer & Saffman (1987), who examined the stability of the closely related problem of a bubble moving in a Hele-Shaw cell.

One of the remaining unresolved issues associated with the boundary-value problem identified by McLean & Saffman was the accuracy of its prediction of λ. This point has been further accentuated by the data of Tabeling & Libchaber (1986) and Tabeling *et al.* (1987), obtained from experiments performed with Hele-Shaw cells having different aspect ratios. They found that λ depends on b^2/W^2 as well as on $(\mu U/\sigma)\, W^2/b^2$, and that $\frac{1}{2}$ does not represent a lower bound for λ. The boundary-value problem identified by McLean & Saffman does not have either of these characteristics.

It has been found that these issues are resolved by including further influences of the thin films on the solid surfaces. Schwartz & DeGregoria (1987) include the presence of the thin films in (1.4), and make better predictions of λ, although somewhat higher than those measured experimentally. Reinelt (1987*b*) includes the effect of the thin films on both (1.3) and (1.4), and makes fairly good predictions of λ. There are reasons to believe that the deviation of his theoretical results from the experimental data at large values of $(\mu U/\sigma)\, W^2/b^2$ is a consequence of the analysis being valid only to $O(b/W)$, as $b/W \to 0$. Thus, it appears that the physics, at least from a modelling perspective, is now well-understood.

Considering the nature of our study, it is appropriate to cite the unusual experimental observations of Kopf-Sill & Homsy (1987, 1988), which consist of very slow moving bubbles, and very narrow viscous fingers, both in Hele-Shaw cells. Recently, Saffman & Tanveer (1989) have speculated about their origins. Based upon an analysis that models the presence of thin films, they concluded that another mechanism must be responsible for such small bubble speeds. They proceed to show that such small speeds are plausible if, in fact, the gas makes direct contact with the solid surfaces, i.e. moving contact lines are present. Since they had no knowledge about the properties of the dynamic contact angle for the particular system of concern, they could not be more definitive. They also conjecture that this may be the explanation for the observed narrow viscous fingers.

The organization of the paper is as follows. In §2 the formulation of the problem is presented. We begin by identifying the scales associated with the *inner region*, the region in the immediate vicinity of the fluid interface, and the *outer region*, the region where most of the viscous fluid is present, away from the fluid interface, where to lowest order (1.1) and (1.2) are appropriate. There are aspects of our presentation which are similar to that of Park & Homsy (1984) and Reinelt (1987*a*), who examine the inner region when thin films are present. However, we do not restrict ourselves to an almost straight fluid interface as do Park & Homsy, and our scaling of the velocity components in the inner region differs from that of Reinelt. Two specific problems are identified, each having the characteristic that both $\mu U/\sigma$ and b/W approach zero. In §2.1, the fast speed viscous fingering problem is formulated, defined by holding the parameter $(\mu U/\sigma)\, W/b$ fixed, as $b/W \to 0$. In §2.2, the slow speed problem is formulated, defined by holding the parameter $(\mu U/\sigma)\, W^2/b^2$ fixed, as $b/W \to 0$. In both cases, the analyses of the inner regions are used to generate two boundary conditions for the equations governing the dynamics of the viscous liquid in the outer region. One of the boundary conditions is (1.3), which is not an approximation when moving contact lines are present. The other boundary condition is similar to the more general version of (1.4), suggested by Saffman & Taylor, containing a term like that introduced by Romero. However, in our case, we can identify the term with a physical property of the system, the contact angle, a parameterization consistent with the present understanding of moving contact line problems. Our solution procedure for both problems, which closely follows those of McLean & Saffman and Vanden-Broeck, is presented in §3. The results appear in §4, and the discussion and conclusions are presented in §5.

2. Formulation

In what follows, the relevant scales and dimensionless equations for both the inner and outer regions are presented. The goal is to obtain a boundary-value problem whose solution describes the shape of the moving contact line.

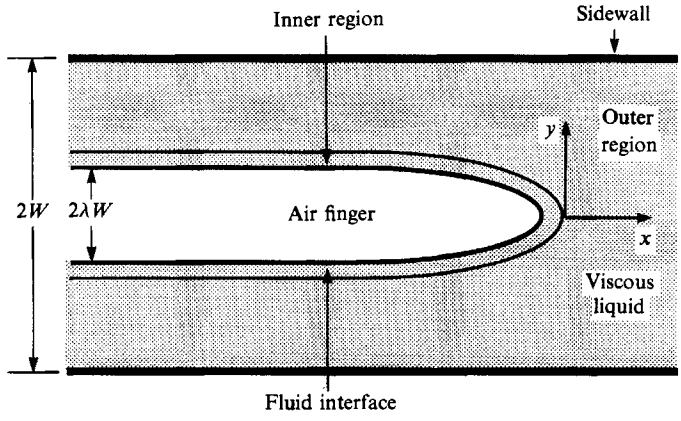

FIGURE 2. A finger of air penetrating a viscous liquid. The inner and outer regions are indicated. The origin for the coordinate system, used to describe the motion of the liquid in the outer region, is located at the nose of the finger. The directions of the x- and y-axes are indicated.

The plane view of a typical finger is given in figure 2. In formulating the problem, the frame of reference is assumed to be at rest with respect to the finger. The origin of the coordinate system for the outer region is fixed at the nose of the finger, located at the centre of the Hele-Shaw cell. The x-axis points in the direction of flow, and the y-axis lies tangent to the solid surfaces and perpendicular to the x-axis. Thus, the cell occupies the domain $\{-\infty < x < +\infty,\ -W \leqslant y \leqslant W,\ -\frac{1}{2}b \leqslant z \leqslant \frac{1}{2}b\}$. As is assumed in other studies, the dynamics of the less viscous fluid, the fluid within the finger, can be neglected. In the outer region, the pressure balances viscous forces induced by velocity variations across the narrow gap of the cell. The dependent and independent variables are denoted by $\bar{P}\mu UW/b^2$, $\bar{V}_x U$, $\bar{V}_y U$, $\bar{V}_z bU/W$, $\bar{x}W$, $\bar{y}W$, and $\bar{z}b$, U being the finger speed. Here, $\bar{P}$ denotes the pressure, $(\bar{V}_x, \bar{V}_y, \bar{V}_z)$ denotes the velocity components, and the overbar denotes variables made dimensionless with the scales appropriate for the outer region. Upon substituting the above into the Navier–Stokes equation, the following dimensionless groups arise: the Reynolds number, $\rho UW/\mu$, denoted by Re; a small parameter, b/W, denoted by ϵ; and $\rho gW^2/\mu U$, where g denotes the gravitational constant. Since the dynamics of the fluid in the outer region is well-known, we only explicitly state the boundary conditions peculiar to the fingering problem:

$$\bar{V} \sim (-6\lambda(\bar{z}^2 - \tfrac{1}{4}) - 1)\,\hat{x} \quad \text{as } \bar{x} \to \infty,$$

$$\bar{V} \sim -\hat{x} \quad \text{as } \bar{x} \to -\infty,$$

$$\bar{V}_y = 0 \quad \text{at } \bar{y} = \pm 1,$$

where $2\lambda W$ denotes the finger width, $\bar{V}$ is the velocity vector, and the circumflex denotes a unit vector.

For the purposes of analysing the inner region, the above defined (x, y, z)-coordinate system is not optimal. Instead, a different coordinate system is developed based upon the contact line shape. The new (X, s, z) orthogonal coordinate system is related to the (x, y, z) system as shown in figure 3, where the variable z is defined as in the outer region. Note that only half of the finger, where $y > 0$, is considered due to the symmetric finger shape. In the inner region, surface tension forces dominate over viscous forces, and the flow field is strongly three-dimensional. Since the no-slip boundary condition is satisfied in the inner region at the top and bottom plates, the velocity components in the X and s directions scale with U. There is no fluid leakage

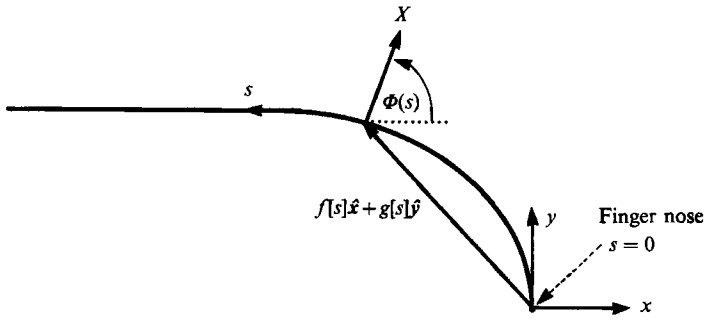

FIGURE 3. Relationship of the coordinate system used in the inner region to the coordinate system used in the outer region. The plan view of the contact-line viscous finger is shown for $y > 0$. The location of the contact line is given by the parameterization $x = f(s)$, $y = g(s)$ in the $X-s-z$ inner-coordinate system. The z-direction is upward and perpendicular to the figure as in the outer region.

into the finger at the contact line, and thus the velocity component in the z-direction also scales with U. The variables X and z scale with b, while s scales with W. The interface parameterization is given by $X = \eta(s, z)$. An important feature of the inner region is that the pressure scales with the surface tension, i.e. σ/b. All variables made dimensionless using these scales are denoted with a tilde, and as before, unit vectors are denoted with a circumflex. Thus, the Navier–Stokes equation and continuity equation in dimensionless form are:

$$Re\,Ca\left\{\epsilon\tilde{\boldsymbol{V}}\cdot\tilde{\boldsymbol{\nabla}}\tilde{V}_X-\epsilon^2\frac{(\tilde{h}_s)}{\tilde{R}}\tilde{V}_s^2\right\}=-\frac{\partial\tilde{P}}{\partial\tilde{X}}+Ca\{\nabla_v^2\tilde{V}_X+\epsilon\tilde{\nabla}_a\tilde{V}_X\}$$

$$+\epsilon^2 Ca\left\{\tilde{\nabla}_b\tilde{V}_X-2\frac{(\tilde{h}_s)^2}{\tilde{R}}\frac{\partial\tilde{V}_s}{\partial\tilde{s}}+\frac{(\tilde{h}_s)^3\tilde{V}_s}{\tilde{R}^2}\frac{\mathrm{d}\tilde{R}}{\mathrm{d}\tilde{s}}\right\}+\epsilon^3 Ca\,\tilde{\nabla}_c\tilde{V}_X,$$

$$Re\,Ca\left\{\epsilon\tilde{\boldsymbol{V}}\cdot\tilde{\boldsymbol{\nabla}}\tilde{V}_s+\epsilon^2\frac{(\tilde{h}_s)}{\tilde{R}}\tilde{V}_s\tilde{V}_X\right\}=-\epsilon(\tilde{h}_s)\frac{\partial\tilde{P}}{\partial\tilde{s}}+Ca\{\nabla_v^2\tilde{V}_s+\epsilon\tilde{\nabla}_a\tilde{V}_s\}$$

$$+\epsilon^2 Ca\left\{\tilde{\nabla}_b\tilde{V}_s+2\frac{(\tilde{h}_s)^2}{\tilde{R}}\frac{\partial\tilde{V}_X}{\partial\tilde{s}}-\frac{(\tilde{h}_s)^3\tilde{V}_X}{\tilde{R}^2}\frac{\mathrm{d}\tilde{R}}{\mathrm{d}\tilde{s}}\right\}+\epsilon^3 Ca\,\tilde{\nabla}_c\tilde{V}_s,$$

$$Re\,Ca\{\epsilon\tilde{\boldsymbol{V}}\cdot\tilde{\boldsymbol{\nabla}}\tilde{V}_z\}=-\frac{\partial\tilde{P}}{\partial\tilde{z}}+Ca\{\tilde{\nabla}_v^2\tilde{V}_z+\epsilon\tilde{\nabla}_a\tilde{V}_z\}+\epsilon^2(\tilde{h}_s)^2\frac{\partial^2\tilde{V}_z}{\partial\tilde{s}^2}+\epsilon^3 Ca\tilde{\nabla}_c\tilde{V}_z-Bd\epsilon^2,$$

$$\frac{\partial\tilde{V}_X}{\partial\tilde{X}}+\frac{\partial\tilde{V}_z}{\partial\tilde{z}}+\epsilon\left\{(\tilde{h}_s)\frac{\partial\tilde{V}_s}{\partial\tilde{s}}+\frac{(\tilde{h}_s)}{\tilde{R}}\tilde{V}_X\right\}=0,$$

where

$$\frac{1}{\tilde{R}}=\frac{\mathrm{d}\Phi}{\mathrm{d}\tilde{s}},\quad \tilde{h}_s=\frac{\tilde{R}}{(\tilde{R}+\epsilon\tilde{X})},\quad \tilde{\boldsymbol{V}}=\tilde{V}_X\hat{\boldsymbol{X}}+\tilde{V}_s\hat{\boldsymbol{s}}+\tilde{V}_z\hat{\boldsymbol{z}},$$

$$\tilde{\boldsymbol{\nabla}}=\frac{\partial}{\partial\tilde{X}}\hat{\boldsymbol{X}}+\epsilon(\tilde{h}_s)\frac{\partial}{\partial\tilde{s}}\hat{\boldsymbol{s}}+\frac{\partial}{\partial\tilde{z}}\hat{\boldsymbol{z}},\quad \tilde{\nabla}_v^2=\left(\frac{\partial^2}{\partial\tilde{X}^2}+\frac{\partial^2}{\partial\tilde{z}^2}\right),\quad \tilde{\nabla}_a=\frac{(\tilde{h}_s)}{\tilde{R}}\frac{\partial}{\partial\tilde{X}},$$

$$\tilde{\nabla}_b=(\tilde{h}_s)^2\frac{\partial^2}{\partial\tilde{s}^2}-\frac{(\tilde{h}_s)^2}{\tilde{R}^2},\quad \tilde{\nabla}_c=\frac{(\tilde{h}_s)^3\tilde{X}}{\tilde{R}^2}\frac{\mathrm{d}\tilde{R}}{\mathrm{d}\tilde{s}}\frac{\partial}{\partial\tilde{s}}.$$

Here, the parameter Ca denotes the capillary number, $\mu U/\sigma$, introduced in §1, and Bd is the Bond number, $\rho g W^2/\sigma$; the angle Φ is defined in figure 3,and $1/\tilde{R}$ shall be

referred to as the spanwise component of the interfacial curvature. The no-slip condition on the upper and lower plates is given by:

$$\tilde{V}_X = -\cos\Phi(s), \quad \tilde{V}_s = \sin\Phi(s), \quad \tilde{V}_z = 0 \quad \text{at } \tilde{z} = \pm\tfrac{1}{2}.$$

The kinematic boundary condition at the fluid interface is given by:

$$\tilde{V}_X = \tilde{V}_z\left(\frac{\partial\tilde{\eta}}{\partial\tilde{z}}\right) + \epsilon\tilde{V}_s\tilde{h}_s\left(\frac{\partial\tilde{\eta}}{\partial\tilde{s}}\right) \quad \text{at } \tilde{X} = \tilde{\eta}(\tilde{s},\tilde{z}).$$

The dynamic boundary condition at the fluid interface is given by:

$$\left\{\frac{\partial\tilde{V}_s}{\partial\tilde{X}} - \frac{\partial\tilde{\eta}}{\partial\tilde{z}}\frac{\partial\tilde{V}_s}{\partial\tilde{z}}\right\} + \epsilon\tilde{h}_s\frac{\partial\tilde{\eta}}{\partial\tilde{s}}\left\{2\frac{\partial\tilde{V}_X}{\partial\tilde{X}} - \frac{\partial\tilde{\eta}}{\partial\tilde{z}}\left(\frac{\partial\tilde{V}_z}{\partial\tilde{X}} + \frac{\partial\tilde{V}_X}{\partial\tilde{z}}\right)\right\} + \epsilon\tilde{h}_s\left\{\frac{\partial\tilde{V}_X}{\partial\tilde{s}} - \frac{\tilde{V}_s}{\tilde{R}} - \frac{\partial\tilde{\eta}}{\partial\tilde{z}}\frac{\partial\tilde{V}_z}{\partial\tilde{s}}\right\}$$
$$-\epsilon^2(\tilde{h}_s)^2\left(\frac{\partial\tilde{\eta}}{\partial\tilde{s}}\right)\left\{\frac{\partial\tilde{\eta}}{\partial\tilde{s}}\frac{\partial\tilde{V}_s}{\partial\tilde{X}} + 2\frac{\partial\tilde{V}_s}{\partial\tilde{s}} + 2\frac{\tilde{V}_X}{\tilde{R}}\right\} + \epsilon^3(\tilde{h}_s)^3\left(\frac{\partial\tilde{\eta}}{\partial\tilde{s}}\right)^2\left\{\frac{\tilde{V}_s}{\tilde{R}} - \frac{\partial\tilde{V}_X}{\partial\tilde{s}}\right\} = 0 \quad \text{at } \tilde{X} = \tilde{\eta}(\tilde{s},\tilde{z}),$$

$$\left\{2\frac{\partial\tilde{\eta}}{\partial\tilde{z}}\left(\frac{\partial\tilde{V}_X}{\partial\tilde{X}} - \frac{\partial\tilde{V}_z}{\partial\tilde{z}}\right) + \left(\frac{\partial\tilde{V}_X}{\partial\tilde{z}} + \frac{\partial\tilde{V}_z}{\partial\tilde{X}}\right)\left(1 - \left(\frac{\partial\tilde{\eta}}{\partial\tilde{z}}\right)^2\right)\right\} - \epsilon\tilde{h}_s\frac{\partial\tilde{\eta}}{\partial\tilde{s}}\left\{\frac{\partial\tilde{\eta}}{\partial\tilde{z}}\frac{\partial\tilde{V}_s}{\partial\tilde{X}} + \frac{\partial\tilde{V}_s}{\partial\tilde{z}}\right\}$$
$$+\epsilon^2(\tilde{h}_s)^2\frac{\partial\tilde{\eta}}{\partial\tilde{s}}\left\{\frac{\partial\tilde{\eta}}{\partial\tilde{z}}\left(\frac{\tilde{V}_s}{\tilde{R}} - \frac{\partial\tilde{V}_X}{\partial\tilde{s}}\right) - \frac{\partial\tilde{V}_z}{\partial\tilde{s}}\right\} = 0 \quad \text{at } \tilde{X} = \tilde{\eta}(\tilde{s},\tilde{z}),$$

$$\frac{1}{2Ca}\left\{\tilde{P} - \frac{1}{\tilde{R}_m}\right\}\left\{1 + \epsilon^2(\tilde{h}_s)^2\left(\frac{\partial\tilde{\eta}}{\partial\tilde{s}}\right)^2 + \left(\frac{\partial\tilde{\eta}}{\partial\tilde{z}}\right)^2\right\} = \left\{\frac{\partial\tilde{V}_X}{\partial\tilde{X}} + \frac{\partial\tilde{V}_z}{\partial\tilde{z}}\left(\frac{\partial\tilde{\eta}}{\partial\tilde{z}}\right)^2 - \frac{\partial\tilde{\eta}}{\partial\tilde{z}}\left(\frac{\partial\tilde{V}_z}{\partial\tilde{X}} + \frac{\partial\tilde{V}_X}{\partial\tilde{z}}\right)\right\}$$
$$+\epsilon\tilde{h}_s\frac{\partial\tilde{\eta}}{\partial\tilde{s}}\left\{\frac{\partial\tilde{\eta}}{\partial\tilde{z}}\frac{\partial\tilde{V}_s}{\partial\tilde{z}} - \frac{\partial\tilde{V}_s}{\partial\tilde{X}}\right\} + \epsilon^2(\tilde{h}_s)^2\frac{\partial\tilde{\eta}}{\partial\tilde{s}}\left\{\frac{\tilde{V}_s}{\tilde{R}} + \frac{\partial\tilde{\eta}}{\partial\tilde{z}}\frac{\partial\tilde{V}_z}{\partial\tilde{s}} - \frac{\partial\tilde{V}_X}{\partial\tilde{s}}\right\}$$
$$+\epsilon^3(\tilde{h}_s)^3\left(\frac{\partial\tilde{\eta}}{\partial\tilde{s}}\right)^2\left\{\frac{\partial\tilde{V}_s}{\partial\tilde{s}} + \frac{\tilde{V}_X}{\tilde{R}}\right\} \quad \text{at } \tilde{X} = \tilde{\eta}(\tilde{s},\tilde{z}),$$

where:

$$\frac{1}{\tilde{R}_m} = \frac{(\partial^2\tilde{\eta}/\partial\tilde{z}^2) + \epsilon A_a + \epsilon^2 A_c + \epsilon^2\tilde{h}_s^2([\partial\tilde{\eta}/\partial\tilde{s}])^2}{\{1 + \epsilon^2(\tilde{h}_s)^2([\partial\tilde{\eta}/\partial\tilde{s}])^2 + ([\partial\tilde{\eta}/\partial\tilde{z}])^2\}^{\frac{3}{2}}},$$

$$A_a(\tilde{s},\tilde{z}) = (\tilde{h}_s)^3\left\{1 + \left(\frac{\partial\tilde{\eta}}{\partial\tilde{z}}\right)^2\right\}\left\{-\frac{1}{\tilde{R}} + \epsilon\left(\frac{\partial^2\tilde{\eta}}{\partial\tilde{s}^2} - 2\frac{\tilde{\eta}}{\tilde{R}^2}\right) + \epsilon^2 A_b(\tilde{s},\tilde{z})\right\},$$

$$A_b(\tilde{s},\tilde{z}) = \frac{1}{\tilde{R}}\left\{-\frac{\tilde{\eta}^2}{\tilde{R}^2} + \frac{\partial\tilde{\eta}}{\partial\tilde{s}}\left(\frac{\tilde{\eta}}{\tilde{R}}\frac{\mathrm{d}\tilde{R}}{\mathrm{d}\tilde{s}} - 2\left(\frac{\partial\tilde{\eta}}{\partial\tilde{s}}\right)^2\right) + \epsilon\frac{\partial^2\tilde{\eta}}{\partial\tilde{s}^2}\right\},$$

$$A_c(\tilde{s},\tilde{z}) = -2(\tilde{h}_s)^3\frac{\partial\tilde{\eta}}{\partial\tilde{s}}\frac{\partial\tilde{\eta}}{\partial\tilde{z}}\left\{\frac{\partial^2\tilde{\eta}}{\partial\tilde{z}\,\partial\tilde{s}}\left(1 + \epsilon\frac{\tilde{\eta}}{\tilde{R}}\right) - \epsilon\frac{1}{\tilde{R}}\frac{\partial\tilde{\eta}}{\partial\tilde{z}}\frac{\partial\tilde{\eta}}{\partial\tilde{s}}\right\}.$$

The boundary condition at the contact line is given by:

$$\frac{\partial\tilde{\eta}}{\partial\tilde{z}} = \mp\left(1 + \epsilon^2(\tilde{h}_s)^2\left(\frac{\partial\tilde{\eta}}{\partial\tilde{s}}\right)^2\right)^{\frac{1}{2}}\cot\Theta \quad \text{at } \tilde{z} = \pm\tfrac{1}{2}, \tag{2.1a}$$

where the contact angle, Θ, is assumed to have a linear dependence on contact line speed; i.e. $\mathrm{d}\Theta/\mathrm{d}U$ is constant,

$$\Theta = \Theta_{\mathrm{R}} - \beta\cos\Phi, \quad \beta = \frac{\mathrm{d}\Theta}{\mathrm{d}U}U, \tag{2.1b}$$

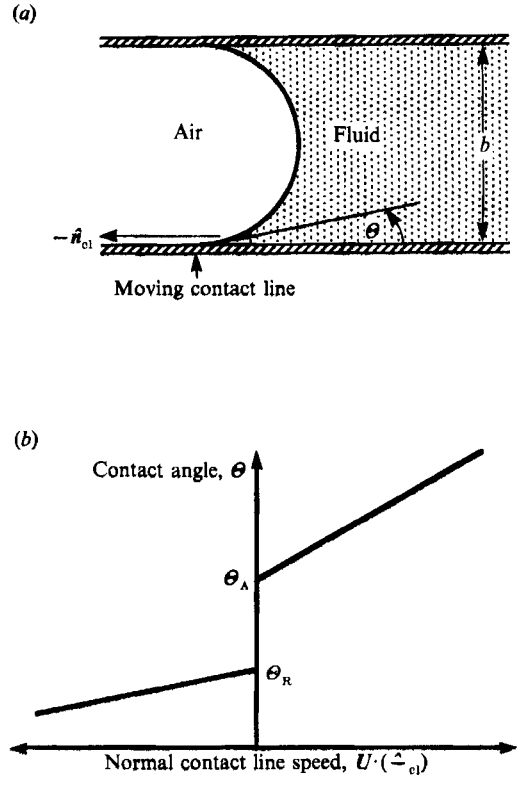

FIGURE 4. The contact angle. (*a*) Cross-sectional view of Hele-Shaw cell in the direction $\hat{n}_{cl}$, perpendicular to the contact line. The contact line and contact angle, Θ, are shown. (*b*) The dependence of contact angle on speed, $V\cdot(-\hat{n}_{cl})$. The contact line is static when $\Theta\in[\Theta_R,\Theta_A]$.

where the local speed of the contact line is given by $U\cos\Phi$ (refer to figure 4).† For the fingering problem, a receding contact line is always present. The two parameters in (2.1*b*) reflect this fact. The first parameter is Θ_R, the receding contact angle, defined to be the smallest static contact angle. Since the speed of the contact line approaches zero as $\Phi\to\frac{1}{2}\pi$, then $\Theta\to\Theta_R$ as $s\to\infty$. The second parameter is β, which incorporates the sensitivity of the contact angle to the speed of the contact line, and affects the magnitude of the angle variation along the contact line. Since the speed of the contact line is $-U$ at $s=0$, it is evident from physical considerations that β must be less than Θ_R. However, it is anticipated that there may be some critical value of β close to Θ_R above which there is a propensity for a thin film to form, and the contact line solution is not physically observed. The solution to this transitional problem is as of yet unsolved.

As stated in §1, the scope of the investigation presented in this paper is limited to situations characterized by the asymptotic limits $\epsilon\to0$ and $Ca\to0$. Two cases will be pursued: Ca/ϵ, β, Re, Bd held fixed as $\epsilon\to0$; and Ca/ϵ^2, β/ϵ, Re, Bd held fixed as

† It is known that the usual hydrodynamic assumptions give rise to a singularity at the moving contact line. In an asymptotic solution, the singularity appears in the expansion of the pressure at $O(Ca)$, as $Ca\to0$. Since we do not analyse in the two specific problems defined below (characterized by holding the parameter Ca/ϵ or Ca/ϵ^2 fixed as ϵ approaches zero) beyond $O(1)$ or $O(\epsilon)$, respectively, we need not specify any additional information concerning the physics of the dynamics of the fluids in the immediate vicinity of the contact line (Ngan & Dussan V. 1989).

$\epsilon \to 0$. These will be referred to as C_1 and C_2 problems, respectively, where $C_1 \equiv Ca/\epsilon$ and $C_2 \equiv Ca/\epsilon^2$. The ratio Ca/ϵ naturally arises in relating the inner and outer pressure scales, since the inner pressure is scaled with the surface tension and the outer pressure is scaled with the viscous forces. These problems can be thought of as representing two different velocity scales. The C_1 problem has the velocity scale given by $\sigma\epsilon/\mu$, while the C_2 problem has a velocity scale given by $\sigma\epsilon^2/\mu$. Thus, the C_1 problem describes fingers moving at a faster speed relative to the C_2 problem. This point of view will be further exploited in §5. There, advantage will be taken of the equivalence of β/C_1 and $\beta/\epsilon C_2$ (alternatively equal to $(\mathrm{d}\theta/\mathrm{d}U)\,\sigma\epsilon/\mu$), and the fact that they depend only upon size of the cell and the material properties of the system. This enables the behaviour of the same material system to be investigated from the perspective of these two different velocity scales.

For each of these problems, surface tension forces dominate viscous forces at the fluid interface; however, the surface tension forces are more important in the lowest-order C_2 problem than in the lowest-order C_1 problem. This difference in surface tension forces is manifested in the way that the spanwise and gapwise variations in the interfacial curvature affect each solution. In the C_1 problem, β is held fixed in the asymptotic limit and thus the contact angle variations along the contact line can be relatively large, inducing large variations in the gapwise interfacial curvature. This means that contact angle variations enter the lowest-order boundary-value problem; the spanwise interfacial curvature enters in higher-order corrections to the contact line shape. On the other hand, in the C_2 problem it is required that β/ϵ is held fixed. Thus, the spanwise and gapwise variations in the curvature along the contact line both play a significant role in determining its shape; both enter the lowest-order boundary-value problem to determine the contact line shape.

2.1. *Ca/ϵ held fixed as $\epsilon \to 0$*

The dimensionless dependent variables defined in the outer region are expanded as:

$$\bar{T} \sim \bar{T}_0(\bar{x}; C_1, \beta, \Theta_R, Re, Bd) + \epsilon \bar{T}_1(\bar{x}; C_1, \beta, \Theta_R, Re, Bd) + \ldots \quad \text{as } \epsilon \to 0,$$

where $\bar{T}$ denotes either $\bar{P}$ or $\bar{V}$, and $\bar{x}$ is the position vector. Using this expansion, the lowest-order outer problem is characterized by Hele-Shaw flow:

$$\frac{\partial^2 \phi_0}{\partial \bar{x}^2} + \frac{\partial^2 \phi_0}{\partial \bar{y}^2} = 0,$$

$$\frac{\partial \phi_0}{\partial \bar{x}} \hat{x} + \frac{\partial \phi_0}{\partial \bar{y}} \hat{y} \to \begin{cases} (\lambda - 1)\,\hat{x} & \text{as } \bar{x} \to \infty \\ -\hat{x} & \text{as } \bar{x} \to -\infty, \end{cases}$$

$$\frac{\partial \phi_0}{\partial \bar{y}} = 0 \quad \text{at } \bar{y} = \pm 1,$$

where: $\phi_0 = -\frac{1}{12}\bar{P}_0(\bar{x}, \bar{y}) - \bar{x}$, $\displaystyle\int_{-\frac{1}{2}}^{\frac{1}{2}} (\bar{V}_{x_0}\hat{x} + \bar{V}_{y_0}\hat{y})\,\mathrm{d}\bar{z} = \frac{\partial \phi_0}{\partial \bar{x}}\hat{x} + \frac{\partial \phi_0}{\partial \bar{y}}\hat{y}$, $\bar{V}_{z_0} = 0$.

The dimensionless dependent variables defined in the inner region are expanded in ϵ as:

$$\tilde{T} \sim \tilde{T}_0(\tilde{x}; C_1, \beta, \Theta_R, Re, Bd) + \epsilon \tilde{T}_1(\tilde{x}; C_1, \beta, \Theta_R, Re, Bd) + \ldots \quad \text{as } \epsilon \to 0,$$

where $\tilde{T}$ denotes $\tilde{P}$, $\tilde{V}$, or $\tilde{\eta}$ and $\tilde{x}$ is the vector of inner spatial coordinates. Using this expansion, the lowest order defined in the inner region is:

$$\frac{\partial \tilde{P}_0}{\partial \tilde{X}} = \frac{\partial \tilde{P}_0}{\partial \tilde{z}} = 0, \tag{2.2}$$

$$\frac{1}{C_1}\frac{\partial \tilde{P}_0}{\partial \tilde{s}} = \frac{\partial^2 \tilde{V}_{s_0}}{\partial \tilde{X}^2} + \frac{\partial^2 \tilde{V}_{s_0}}{\partial \tilde{z}^2}, \tag{2.3}$$

$$\frac{1}{C_1}\frac{\partial \tilde{P}_1}{\partial \tilde{X}} = \frac{\partial^2 \tilde{V}_{X_0}}{\partial \tilde{X}^2} + \frac{\partial^2 \tilde{V}_{X_0}}{\partial \tilde{z}^2}, \tag{2.4}$$

$$\frac{1}{C_1}\frac{\partial \tilde{P}_1}{\partial \tilde{z}} = \frac{\partial^2 \tilde{V}_{z_0}}{\partial \tilde{X}^2} + \frac{\partial^2 \tilde{V}_{z_0}}{\partial \tilde{z}^2}, \tag{2.5}$$

$$\frac{\partial \tilde{V}_{X_0}}{\partial \tilde{X}} + \frac{\partial \tilde{V}_{z_0}}{\partial \tilde{z}} = 0, \tag{2.6}$$

$$\tilde{V}_{X_0} = -\cos \Phi_0 \quad \text{at } \tilde{z} = \pm\tfrac{1}{2}, \tag{2.7}\dagger$$

$$\tilde{V}_{z_0} = 0 \quad \text{at } \tilde{z} = \pm\tfrac{1}{2}, \tag{2.8}$$

$$\tilde{V}_{s_0} = \sin \Phi_0 \quad \text{at } \tilde{z} = \pm\tfrac{1}{2}, \tag{2.9}$$

$$\frac{\partial \tilde{\eta}_0}{\partial \tilde{z}} = \mp \cot(\Theta_R - \beta \cos \Phi_0) \quad \text{at } \tilde{z} = \pm\tfrac{1}{2}, \tag{2.10}$$

$$\tilde{V}_{X_0} = \tilde{V}_{z_0}\frac{\partial \tilde{\eta}_0}{\partial \tilde{z}} \quad \text{at } \tilde{X} = \tilde{\eta}_0(\tilde{s}, \tilde{z}), \tag{2.11}$$

$$\frac{\partial \tilde{V}_{s_0}}{\partial \tilde{X}} = \frac{\partial \tilde{\eta}_0}{\partial \tilde{z}}\frac{\partial \tilde{V}_{s_0}}{\partial \tilde{z}} \quad \text{at } \tilde{X} = \tilde{\eta}_0(\tilde{s}, \tilde{z}), \tag{2.12}$$

$$2\frac{\partial \tilde{\eta}_0}{\partial \tilde{z}}\left\{\frac{\partial \tilde{V}_{X_0}}{\partial \tilde{X}} - \frac{\partial \tilde{V}_{z_0}}{\partial \tilde{z}}\right\} + \left\{\frac{\partial \tilde{V}_{X_0}}{\partial \tilde{z}} + \frac{\partial \tilde{V}_{z_0}}{\partial \tilde{X}}\right\}\left\{1 - \left(\frac{\partial \tilde{\eta}_0}{\partial \tilde{z}}\right)^2\right\} = 0 \quad \text{at } \tilde{X} = \tilde{\eta}_0(\tilde{s}, \tilde{z}), \tag{2.13}$$

$$\tilde{P}_0 = \frac{(\partial^2 \tilde{\eta}_0/\partial \tilde{z}^2)}{\{1 + ([\partial \tilde{\eta}_0/\partial \tilde{z}])^2\}^{\frac{3}{2}}} \quad \text{at } \tilde{X} = \tilde{\eta}_0(\tilde{s}, \tilde{z}). \tag{2.14}$$

Integrating (2.14) (noting that (2.2) and (2.3) imply that $\tilde{P}$ can at most depend on s), and using the contact angle condition (2.10), the solution for the lowest-order inner region pressure is:

$$\tilde{P}_0 = -2\cos(\Theta_R - \beta \cos \Phi_0) \quad \forall \tilde{X}, \tilde{z}$$

Note that the angle Φ_0 is a function of $\tilde{s}$, yet to be determined. The remaining equations, (2.4)–(2.8), (2.11) and (2.13), indicate that:

$$\int_{-\frac{1}{2}}^{\frac{1}{2}} \tilde{V}_{X_0}\, d\bar{z} \to 0 \quad \text{as } \tilde{X} \to \infty,$$

where the integral gives the speed averaged across the gap. Matching the inner and outer regions thus leads to the following boundary-value problem:

$$\frac{\partial^2 \phi_0}{\partial \bar{x}^2} + \frac{\partial^2 \phi_0}{\partial \bar{y}^2} = 0, \tag{2.15a}$$

† It should be noted that Φ_0 denotes the lowest-order location of the contact line. The coordinates system is based on this lowest-order shape; thus, there are no higher-order corrections to boundary conditions (2.7) and (2.9).

$$\frac{\partial \phi_0}{\partial \bar{y}} = 0 \quad \text{at } \bar{y} = \pm 1, \tag{2.15b}$$

$$\bar{\nabla}\phi_0 \cdot \hat{n}_{cl_0} = 0 \quad \text{at } \bar{x} = \bar{f}_0(\bar{y}), \tag{2.15c}$$

$$\phi_0 = \frac{1}{6C_1}\cos(\Theta_R - \beta\cos\Phi_0) - \bar{x} \quad \text{at } \bar{x} = \bar{f}_0(\bar{y}), \tag{2.15d}$$

$$\bar{\nabla}\phi_0(\bar{x}, \bar{y}) \to (\lambda - 1)\hat{x} \quad \text{as } \bar{x} \to \infty, \tag{2.15e}$$

$$\bar{\nabla}\phi_0(\bar{x}, \bar{y}) \to -\hat{x} \quad \text{as } \bar{x} \to -\infty. \tag{2.15f}$$

In (2.15*c*) and (2.15*d*), the shape of the contact line, to be determined as part of the solution, is parameterized as $\bar{x} = \bar{f}_0(\bar{y})$. Note that the curve also represents the shape of the finger in the $\bar{z} = 0$ plane, since the difference between that and the moving contact line is of $O(\epsilon)$.

2.2. *Ca/ϵ^2 held fixed as $\epsilon \to 0$*

The expansion of the dimensionless dependent variables and their governing equations for the outer region in the C_2 problem are identical to those for the C_1 problem, except that the pressure contains a new lowest-order term:

$$\bar{P} \sim \epsilon^{-1}\bar{P}_{-1} + \bar{P}_0\left(\bar{x}; C_2, \frac{\beta}{\epsilon}, \Theta_R, Re, Bd\right) + \epsilon\bar{P}_1\left(\bar{x}; C_2, \frac{\beta}{\epsilon}, \Theta_R, Re, Bd\right) + \ldots \quad \text{as } \epsilon \to 0,$$

where it can be shown that $\bar{P}_{-1}$ is a constant. The dimensionless dependent variables defined in the inner region are expanded in a similar manner to that in the C_1 problem:

$$\tilde{T} \sim \tilde{T}_0\left(\bar{x}; C_2, \frac{\beta}{\epsilon}, \Theta_R, Re, Bd\right) + \epsilon\tilde{T}_1\left(\bar{x}; C_2, \frac{\beta}{\epsilon}, \Theta_R, Re, Bd\right) + \ldots \quad \text{as } \epsilon \to 0.$$

The major difference between the C_1 and C_2 problems in the inner region equations lies in the equations to solve for the pressure. It is necessary to solve for $\tilde{P}_0$ as well as $\tilde{P}_1$ in order to completely determine $\bar{P}_0$ and the shape of the contact line to lowest order. The lowest-order problem in the inner region is given by:

$$\frac{\partial \tilde{P}_0}{\partial \tilde{X}} = \frac{\partial \tilde{P}_0}{\partial \tilde{s}} = \frac{\partial \tilde{P}_0}{\partial \tilde{z}} = 0, \tag{2.16}$$

$$\frac{\partial \tilde{\eta}_0}{\partial \tilde{z}} = \mp \cot\Theta_R \quad \text{at } \tilde{z} = \pm\tfrac{1}{2}, \tag{2.17}$$

$$\tilde{P}_0 = \frac{(\partial^2\tilde{\eta}_0/\partial\tilde{z}^2)}{\{1 + ([\partial\tilde{\eta}_0/\partial\tilde{z}])^2\}^{\frac{3}{2}}}. \tag{2.18}$$

It is evident that $\tilde{P}_0$ is an absolute constant, given by:

$$\tilde{P}_0 = -2\cos\Theta_R. \tag{2.19}$$

The next order problem is given by:

$$\frac{\partial \tilde{P}_1}{\partial \tilde{X}} = \frac{\partial \tilde{P}_1}{\partial \tilde{z}} = 0, \tag{2.20}$$

$$\frac{\partial \tilde{\eta}_1}{\partial \tilde{z}} = \mp (\mathrm{cosec}^2\Theta_R)\gamma\cos\Phi_0 \quad \text{at } \tilde{z} = \pm\tfrac{1}{2}, \tag{2.21}$$

$$\tilde{P}_1(\tilde{s}) = \frac{\partial}{\partial\tilde{z}}\left(\frac{(\partial\tilde{\eta}_1/\partial\tilde{z})}{\{1 + ([\partial\tilde{\eta}_0/\partial\tilde{z}])^2\}^{\frac{1}{2}}}\right) - \frac{(\mathrm{d}\Phi_0/\mathrm{d}\tilde{s})}{\{1 + ([\partial\tilde{\eta}_0/\partial\tilde{z}])^2\}^{\frac{1}{2}}}, \tag{2.22}$$

where $\gamma \equiv \beta/\epsilon$. Evaluating $\partial\tilde{\eta}_0/\partial\tilde{z}$ using (2.17), (2.18) and (2.19) gives:

$$\frac{\partial\tilde{\eta}_0}{\partial\tilde{z}} = \frac{-2\tilde{z}\cos\Theta_R}{(1-4\tilde{z}^2\cos^2\Theta_R)^{\frac{1}{2}}} \tag{2.23}$$

Substituting (2.23) into (2.22) and integrating once with respect to $\tilde{z}$ gives:

$$\tilde{P}_1 = -2\gamma\sin\Theta_R\cos\Phi_0 - \delta\frac{d\Phi_0}{d\bar{s}} \quad \forall\tilde{X},\tilde{z}, \tag{2.24}$$

where:

$$\delta = \frac{\sin 2\Theta_R + \pi - 2\Theta_R}{4\cos\Theta_R}. \tag{2.25}$$

Matching the inner and outer pressures thus yields:

$$\bar{P} \sim \frac{-2\epsilon^{-1}}{C_2}\cos\Theta_R - \frac{1}{C_2}\left[2\gamma\sin\Theta_R\cos\Phi_0 + \delta\frac{d\Phi_0}{d\bar{s}}\right] + \ldots \tag{2.26}$$

The $O(1)$ term in (2.26) interacts with the lowest-order flow in the outer region to determine the shape of the contact line. The C_2 lowest-order outer boundary-value problem is identical to that for the C_1 problem, given by (2.15), where the potential along the finger shape, (2.15*d*), is replaced with:

$$\phi_0 = \frac{1}{12C_2}\left[2\gamma\sin\Theta_R\cos\Phi_0 + \delta\frac{d\Phi_0}{d\bar{s}}\right] - \bar{x} \quad \text{at } \bar{x} = \bar{f}_0(\bar{y}). \tag{2.27}$$

The C_1 and C_2 problems are characterized by the differing forms of the interfacial potentials along the fluid interface, (2.15*d*) and (2.27). In the C_1 problem all pressure variations along the fluid interface from the perspective of the outer region is due to changes in the contact angle along the contact line. These angle variations induce variations in the gapwise interface shape. In the C_2 problem, there are two terms contributing to the variation of pressure along the interface. The first term on the right-hand side of (2.27) incorporates the effect of the dynamic contact angle. The second term in (2.27) is the spanwise component of the curvature of the interface. In the C_1 problem, the spanwise component of the curvature enters at $O(\epsilon)$, and thus does not contribute to the lowest-order contact line shape. By comparing the shapes of the contact line in the C_1 and C_2 problems, the consequence of each component of the interfacial curvature can be assessed.

3. Solution procedure

The contact line shape for the viscous finger can be found by solving (2.15) for the C_1 and C_2 problems (for the C_2 problem, replace (2.15*d*) with (2.27)) using the technique outlined in McLean & Saffman (1981) and Vanden-Broeck (1983). Note that the C_2 boundary-value problem reduces to their problem for the finger shape by setting $\gamma = 0$ and $\Theta_R = \frac{1}{2}\pi$ (i.e. removing any variation in the gapwise curvature along the contact line). The power of the technique lies in transforming the two-dimensional free-surface problem where the domain is not known *a priori* to a one-dimensional problem. Following the notation of McLean & Saffman, the contact line shape can be obtained by finding q, the magnitude of the fluid speed in the direction parallel to the contact line, and θ, the local slope of the contact line, where:

$$\theta \equiv \Phi_0 - \tfrac{1}{2}\pi.$$

The boundary-value problem to solve for the contact line shape is given by:

$$\log q = -\frac{1}{\pi} PV \int_0^1 \frac{\theta(s')\,\mathrm{d}s'}{s'-s} + \log(1-\lambda) \quad \forall s \in [0,1], \tag{3.1a}$$

$$\log(1-\lambda) = \frac{1}{\pi}\int_0^1 \frac{\theta(s')\,\mathrm{d}s'}{s'}, \tag{3.1b}$$

$$\theta = -\tfrac{1}{2}\pi, \quad q = 0 \quad \text{at } s = 1, \tag{3.1c, d}$$

$$\theta = 0, \quad q = 1 \quad \text{at } s = 0, \tag{3.1e, f}$$

where q is given by:

$$q = \alpha\beta \sin(\Theta_{\mathrm{R}} + \beta \sin\theta)\, sq \cos\theta \frac{\mathrm{d}\theta}{\mathrm{d}s} + \cos\theta, \tag{3.2a}$$

with:

$$\alpha = \frac{\pi}{6C_1(1-\lambda)}, \quad \beta = \frac{\mathrm{d}\Theta}{\mathrm{d}U} U, \tag{3.2b}$$

in the C_1 problem, and

$$q = K\delta\, sq \frac{\mathrm{d}}{\mathrm{d}s}\left\{sq \frac{\mathrm{d}\theta}{\mathrm{d}s}\right\} + \varpi\, sq \cos\theta \frac{\mathrm{d}\theta}{\mathrm{d}s} + \cos\theta, \tag{3.3a}$$

with:

$$\varpi = \frac{\pi\gamma \sin\Theta_{\mathrm{R}}}{6C_2(1-\lambda)}, \quad K = \frac{\pi^2}{12C_2(1-\lambda)^2}, \tag{3.3b}$$

in the C_2 problem. Here, s is a scaled arc length ranging from 0 at the finger tail to 1 at the finger nose.

The above equations and boundary conditions represent a well-posed system to determine q and θ. Using these results, the shape of the contact line is given by:

$$\bar{x}(s) = \frac{1-\lambda}{\pi}\int_1^s \frac{\cos\theta\,\mathrm{d}s'}{s'q}, \tag{3.4a}$$

$$\bar{y}(s) = \frac{1-\lambda}{\pi}\int_1^s \frac{\sin\theta\,\mathrm{d}s'}{s'q}. \tag{3.4b}$$

A self-consistency check on the value of λ predicted by (3.1*b*) is obtained by noting that $\bar{y}(0) = \lambda$. It should be noted that although (3.3*a*) has higher-order derivatives than (3.2*a*), the C_1 problem is not overspecified with the four conditions (3.1*c*)–(3.1*f*). This is because there is a weak specification of the boundary conditions at the endpoints of the domain. In fact it is only necessary to specify either (3.1*c*) or (3.1*d*), and either (3.1*e*) or (3.1*f*) for a well posed problem to arise (Weinstein 1988).

There are two issues to be addressed in obtaining the solution. The first is whether reasonable contact line shapes are predicted. The second, and not totally unrelated issue, is whether the solutions are unique. The procedure for solving the above set of equations consists of specifying the value of λ while ignoring (3.1*c*) or (3.1*d*). The slope of the finger at its nose can then be calculated as part of the solution to the problem. Whenever the condition (3.1*c*) is satisfied, a solution has been identified. By performing this calculation for all values of λ within the interval $\lambda \in [0,1]$, the subset of λ corresponding to solutions can be identified. If this subset contains more than one element, then the solution is not unique.

More specifically, solutions for the C_1 problem are obtained as follows. Specify C_1, β, Θ_R, and λ_i, the initial value of λ. Calculate α using (3.2*b*). Solve for θ and q using (3.1) and (3.2). When $\theta(1) = -\frac{1}{2}\pi$ is satisfied, a solution is found. The contact line shape is then given by (3.4). Increment λ, and repeat the procedure again, until λ is close to 1. For the C_2 problem, specify C_2, γ, Θ_R, and λ_i. Calculate K, ϖ, and δ using (3.3*b*) and (2.25) and continue with the same procedure as outlined for the C_1 problem.

In order to simplify the determination of the solution numerically, the behaviour of the solution is investigated analytically near the endpoints $s = 0$ and $s = 1$ so it can be scaled out at these locations. The variable transformation employed by Vanden-Broeck (1983) is found to scale out the endpoint singularities and assure sufficient differentiability at the endpoints:

$$s^\tau = (1-\zeta^4) \tag{3.5}$$

McLean & Saffman (1981) use variable transformation given by $s^\tau = (1-\zeta^2)$, as opposed to the form given in (3.5). In their approach, this transformation assures differentiability at $s = 1$, where a square root singularity is present. In the approach of Vanden-Broeck (1983), the calculated value of θ at $s = 1$ determines the severity of the singularity at the finger nose, and it is thus necessary to increase the exponent of ζ to assure differentiability. The exponent τ in (3.5) is determined from the asymptotic behaviour of the solution as $s \to 0$, following techniques presented in McLean & Saffman (1981). For the C_1 problem, it is given by:

$$\cot(\pi\tau) = \alpha\beta \sin(\Theta_R)\,\tau, \tag{3.6}$$

while for the C_2 problem, τ is given by solving:

$$\cot(\pi\tau) = K\delta\tau^2 + \varpi\tau. \tag{3.7}$$

In either case, $\tau \in (0, \frac{1}{2})$. Thus, the singularity exponent τ must be determined each time λ is incremented since the parameters in (3.6) and (3.7) will change.

The same numerical procedure outlined in Vanden-Broeck is used to solve the equations for the C_1 and C_2 problems. A forward difference, finite difference approximation is used to evaluate all derivatives, while the trapezoidal rule is used to evaluate the transformed form of the principal value integral (3.1*a*). Newton's method is then utilized to solve the resultant set of algebraic solutions. In implementing Newton's method, it is necessary to begin with a reasonable guess for the shape of the contact line. It is possible to start with $\lambda = 0$, where all the discretized values of θ equal 0 (which corrresponds to the line $\bar{y} = 0$); these values satisfy the equations exactly. This result is used as an initial guess for the contact line shape at the first incremented value of $\lambda > 0$. Thereafter, as λ is further incremented, the previously converged solution is used as an initial guess for the contact line shape at the new value of λ. The results of the C_2 problem can be directly compared with the results of McLean & Saffman (1981) and Vanden-Broeck (1983) when $\Theta_R = \frac{1}{2}\pi$ and $\varpi = 0$.

Solutions were obtained for both the C_1 and C_2 problems with $N = 60$, $N = 120$, and $N = 240$ segments for a wide range of parameter choices. The $N = 120$ case was deemed accurate enough for the purposes of this work, where the calculated values of the slope at the finger nose, $\theta(1)$, were accurate to 2 decimal places at each value of the finger width, λ. Newton's method converged quadratically in 4–5 iterations at every specified value of λ, provided the increment in λ was not too large to cause

divergence (large increments made initial guesses based upon the previously converged solutions poor).

4. Results

4.1. *The C_1 problem*

The solid line in figure 5(*a*) gives typical results of the C_1 problem. The dotted line indicates $\theta(1) = -\frac{1}{2}\pi$. Thus, the values of λ corresponding to positions where the solid crosses the dotted line represents solutions. Figure 5(*a*) indicates that there exist an infinite continuous set of finger widths for which interface solutions can be found. Since the approximations used in the numerical analysis cease to be valid when $1-\lambda = O(\epsilon)$, it could not be verified that the continuous spectrum of solutions extends to $\lambda = 1$. The distinguishing feature of figure 5(*a*) is the minimum finger width, denoted by λ_m, below which no solutions exist. In figure 5(*a*), $\lambda_m = 0.30$. The range of finger widths for which solutions exist in figure 5(*a*) is thus given by $\lambda \in [0.30, 0.96]$. In figure 5(*b*), the contact line shapes corresponding to $\lambda_m = 0.30$, as well as $\lambda = 0.50$, 0.70 and 0.90 are plotted. These are representative predictions of the continuous spectrum of shapes.

A vital issue is whether the dotted line is ever reached by the numerical results in figure 5(*a*), since these results never cross the line. To verify that values of $\lambda \geqslant \lambda_m$ actually corresponded to solutions, the problem was posed where λ was calculated instead of specified, as was done in McLean & Saffman (1981). Initial guesses were varied in the numerical procedure, and indeed solutions, very close together, were obtained. The distance between these solutions was limited by the finite difference discretization; as the number of discretizations increased, the solutions became closer together. It was observed that no interface solutions were found below a value of λ of approximately 0.3, and so it was concluded that solutions exist for all $\lambda \geqslant \lambda_m$.

The behaviour of the system under different conditions can be determined by evaluating the dependence of λ_m on the three parameters β, β/C_1, and Θ_R. We choose these parameters, as opposed to C_1, β, and Θ_R, to present the results because it facilitates the interpretation of a 'thought' experiment in which the geometrical and material properties are held fixed, while the speed of the finger is varied. This formally corresponds to the case where β/C_1 (equivalent to $(\mathrm{d}\Theta/\mathrm{d}U)\sigma\epsilon/\mu$) and Θ_R are fixed, while β is varied. The parameters β/C_1 and β can be regarded as reflecting the relative importance of dynamic contact angle to viscous forces, and as a dimensionless finger speed, respectively. The parameter β can also be interpreted as a dimensionless angle. When interpreted in this way, parameter values will be given in degrees, and when interpreted as a dimensionless speed, values will be given in radians.

Recall that for a given Θ_R there is a physical bound on the size of β. From the linear contact angle relationship (2.1*b*), it can be seen that in order for contact angles to be non-negative, $\beta \leqslant \Theta_R$. For a fixed material system, this restriction amounts to an upper bound on the finger speed such that a contact line solution exists. However, this does not necessarily represent the least upper bound since the system may be unstable at this speed, resulting in the appearance of a thin film.

Figure 6 shows the results for $\beta/C_1 = 0.05$ and $\Theta_R = 90°$ for β varying from 0.01 to 1.50 radians (0.57° to 89.94°). Curve *B* in this figure is the plot of data shown in figure 5(*a*). It should be noted that β was not evaluated to its upper bound of 1.57 owing to convergence problems with Newton's method. Note that the curves for $\beta = 0.1$ and $\beta = 0.01$ are coincident, indicating an insensitivity of λ_m to β as $\beta \to 0$.

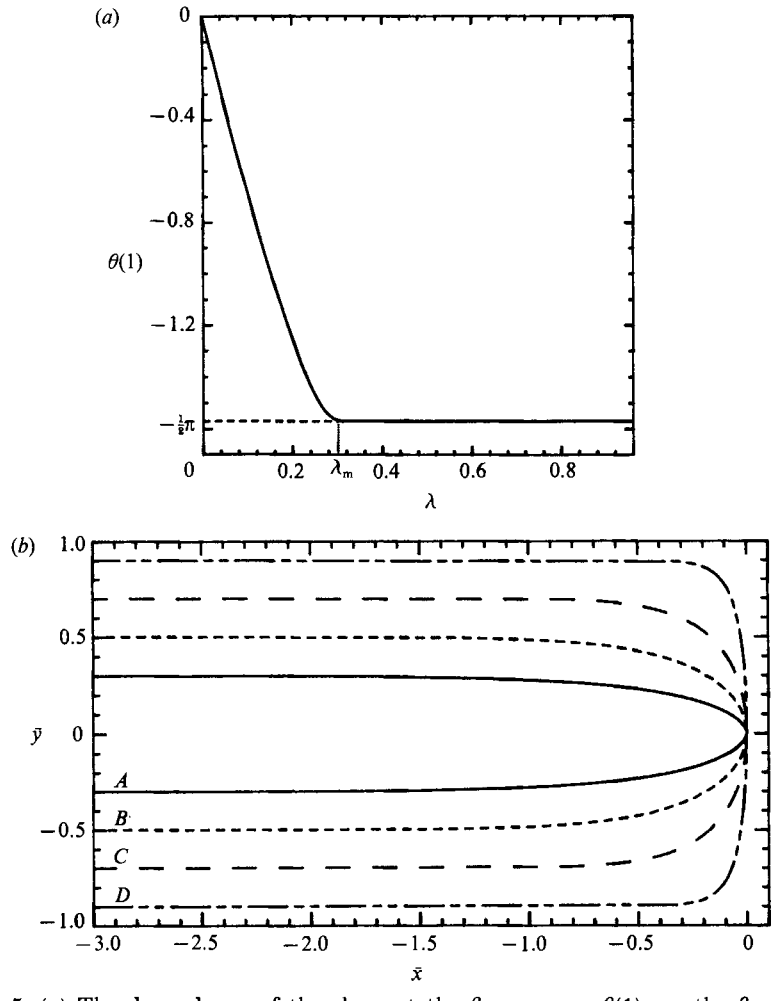

FIGURE 5. (*a*) The dependence of the slope at the finger nose, $\theta(1)$, on the finger width, λ, for $C_1 = 0.2$, $\beta = 0.01$ and $\Theta_R = 90°$. The minimum allowable finger width is $\lambda_m = 0.30$. (*b*) Finger shapes corresponding to finger widths from (*a*), where $C_1 = 0.2$, $\beta = 0.01$ and $\Theta_R = 90°$. A: $\lambda_m = 0.3$; B: $\lambda = 0.5$; C: $\lambda = 0.7$; D: $\lambda = 0.9$.

Physically, the $\beta \to 0$ limit corresponds to the limit of small contact angle dependence on the contact line speed, resulting in small contact angle variations along the contact line. This insensivity at small values of β is expected from the form of (3.2*a*), where β/C_1 is the only remaining parameter for a given material system as $\beta \to 0$. It can thus be seen in figure 6 that for a given value of β/C_1, there exists a band of values of λ_m ranging from about 0.15 to about 0.30, corresponding to β values of 1.57 and 0.01, respectively.

Figure 7 shows the effect of varying Θ_R on the band given by $\{\lambda_m | 0 < \beta < \Theta_R\}$ evaluated for $\beta/C_1 = 0.5$, which we will regard as the representative case. Note that when $\beta \approx \Theta_R$, for this curve, the contact angle at the finger nose is approximately zero. On the other hand when $\beta \approx 0$, the contact angle at the nose, and for that matter along the contact line, is given approximately by Θ_R. Another interesting feature to note is that as Θ_R is increased past approximately 160°, the values of λ_m corresponding to $\beta \approx 0$ lie below those for $\beta = \Theta_R$. This indicates that finger widths

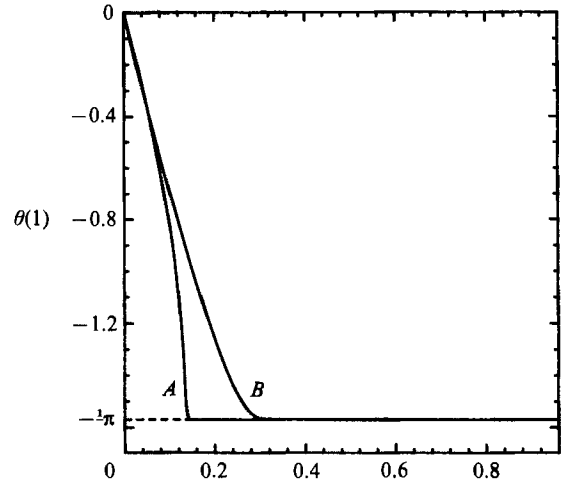

FIGURE 6. The dependence of the slope at the finger nose, $\theta(1)$, on the finger width, λ, for $\beta/C_1 = 0.05$ and $\Theta_R = 90°$. A: $\beta = 1.5$, $\lambda_m = 0.15$; B: $\beta = 0.1$ or 0.01, $\lambda_m = 0.3$.

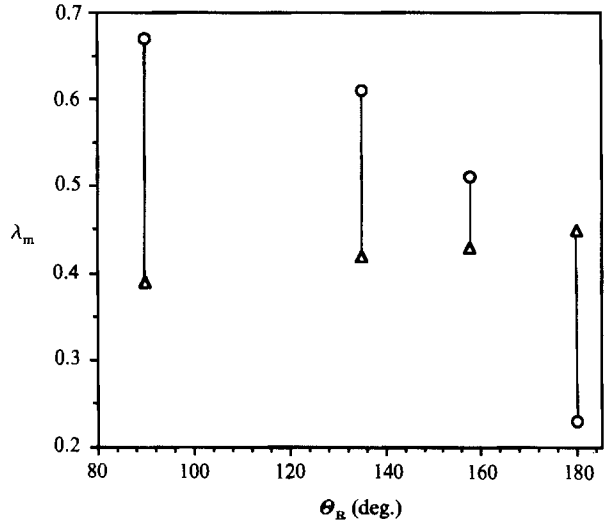

FIGURE 7. The dependence of the finger width, λ_m, on the receding contact angle, Θ_R, for $\beta/C_1 = 0.5$. ○, $\beta \approx 0$; △, $\beta \approx \Theta_R$.

increase as the finger speed is increased, exactly the opposite behaviour to when $\beta < 160°$. When $\Theta_R = 160°$, finger widths are identical for all values of β, i.e. all fluid speeds; however, the finger shapes corresponding to different fluid speeds are different.

4.2. *The C_2 problem*

Figure 8 gives typical results for the C_2 problem. Every time the plot crosses the horizontal dotted line, a value of λ corresponding to a solution is identified. Note that the range of finger widths for $\lambda \in [0, 0.5]$ yields no solutions and thus is not presented. Three values of λ corresponding to solutions are indicated in figure 8. Let the smallest finger width be denoted by λ_0, the next largest denoted by λ_1, and the last value by λ_2. It should be noted that additional solutions appear to exist for $\lambda > 0.88$, but it takes an increasing number of finite difference points to resolve more solutions as λ

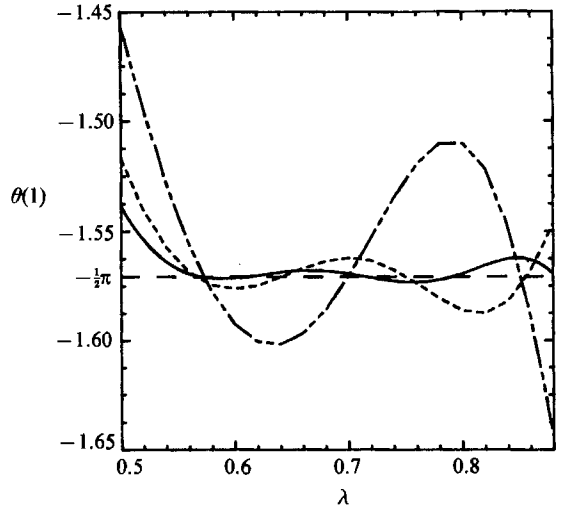

FIGURE 8. The dependence of the slope at the finger nose, $\theta(1)$, on the finger width, λ, for $\gamma/C_2 = 0.05$ and $\Theta_R = 90°$. ——, $C_2 = 120$; - - - - -, $C_2 = 80$; — — —, $C_2 = 40$.

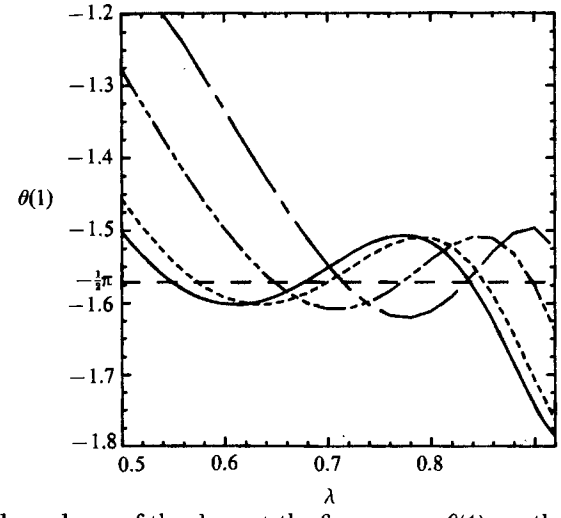

FIGURE 9. The dependence of the slope at the finger nose, $\theta(1)$, on the finger width, λ, for $C_2 = 40$ and $\Theta_R = 90°$. ——, $\gamma = 0$, $\lambda_0 = 0.55$, $\lambda_1 = 0.68$, $\lambda_2 = 0.84$; - - - - -, $\gamma = 2$, $\lambda_0 = 0.57$, $\lambda_1 = 0.70$, $\lambda_2 = 0.85$; — · —, $\gamma = 10$, $\lambda_0 = 0.65$, $\lambda_1 = 0.77$, $\lambda_2 = 0.90$; — — —, $\gamma = 20$, $\lambda_0 = 0.71$, $\lambda_1 = 0.83$.

approaches 1. The difference in values of successive λ corresponding to the oscillations about the dotted line in figure 8 eventually decrease as more and more solutions are found, while the amplitude of the curve increases. Whether or not there exists an infinite discrete set of solutions for the specified parameter values has not been pursued; however, based upon the data trends, one might suspect this to be the case.

The results of the C_2 problem are examined in §5 from two perspectives. One perspective is similar to that used in the C_1 problem, and consists of analysing the solution in terms of the parameters C_2, γ/C_2, and Θ_R. Note that γ/C_2 is identical to β/C_1. The other perspective consists of holding C_2 and Θ_R fixed, while varying the value of γ (refer to figure 9). This facilitates an examination of the relative influences of the gapwise and spanwise curvatures (refer to (2.27)) on the viscous fingering

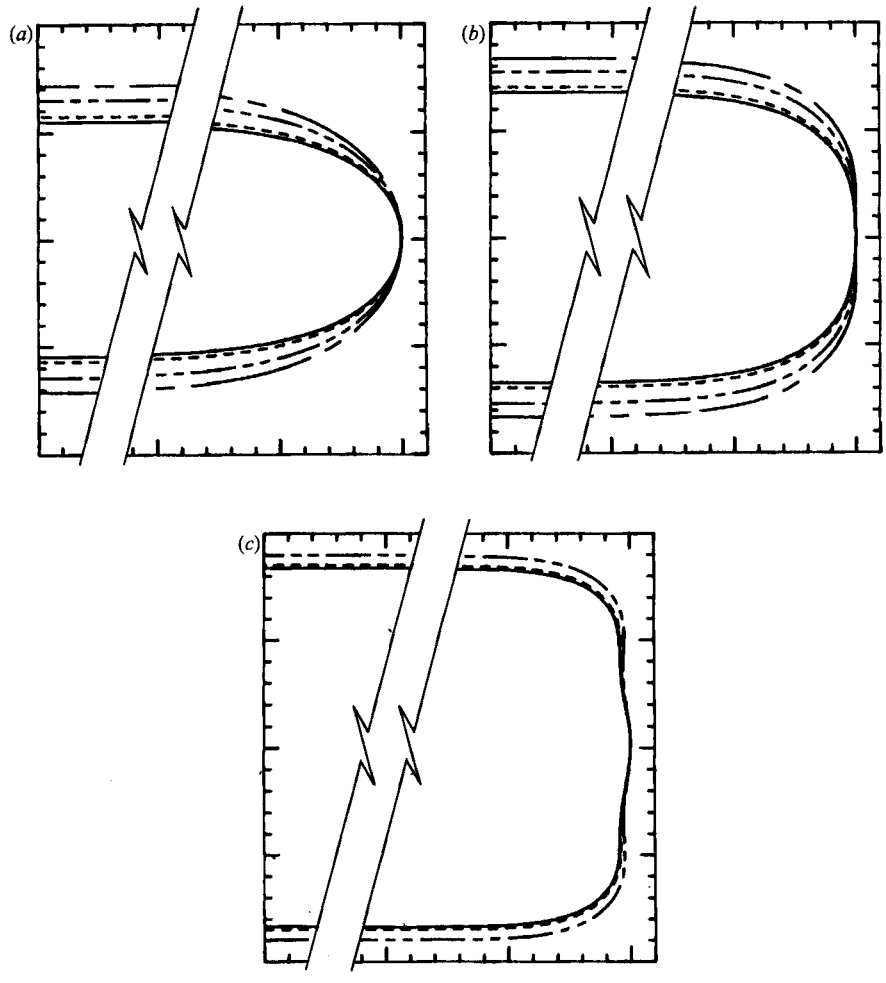

FIGURE 10. (*a*) Finger shapes corresponding to λ_0 values from figure 9, where $C_2 = 40$ and $\Theta_R = 90°$. ——, $\gamma = 0$, $\lambda_0 = 0.55$; - - - - -, $\gamma = 2$, $\lambda_0 = 0.57$; — · —, $\gamma = 10$, $\lambda_0 = 0.65$; — · —, $\gamma = 20$, $\lambda_0 = 0.71$. (*b*) Finger shapes corresponding to λ_1 values from figure 9, where $C_2 = 40$ and $\Theta_R = 90°$. ——, $\gamma = 0$, $\lambda_1 = 0.68$; - - - - -, $\gamma = 2$, $\lambda_1 = 0.70$; — · —, $\gamma = 10$, $\lambda_1 = 0.77$; — · —, $\gamma = 20$, $\lambda_0 = 0.83$. (*c*) Finger shapes corresponding to λ_2 values from figure 9, where $C_2 = 40$ and $\Theta_R = 90°$. ——, $\gamma = 0$, $\lambda_2 = 0.84$; - - - - -, $\gamma = 2$, $\lambda_2 = 0.85$; — · —, $\gamma = 10$, $\lambda_2 = 0.90$.

problem. The contact line shapes corresponding to λ_0, λ_1 and λ_2 are plotted in figures 10(*a*), (*b*) and (*c*), respectively.

5. Discussion and conclusions

It is evident that the presence of moving contact lines do not remove the appearance of multiple solutions from the viscous fingering problem. Although a rigorous mathematical demonstration will not be presented, we shall argue that the physically relevant solutions correspond to λ_m for the C_1 problem, and λ_0 for the C_2 problem. Our approach consists of drawing general conclusions from specific examples, and from making analogies to the well-studied case when a thin film of liquid remains on the solid. Finally, we discuss the similarities between the new class

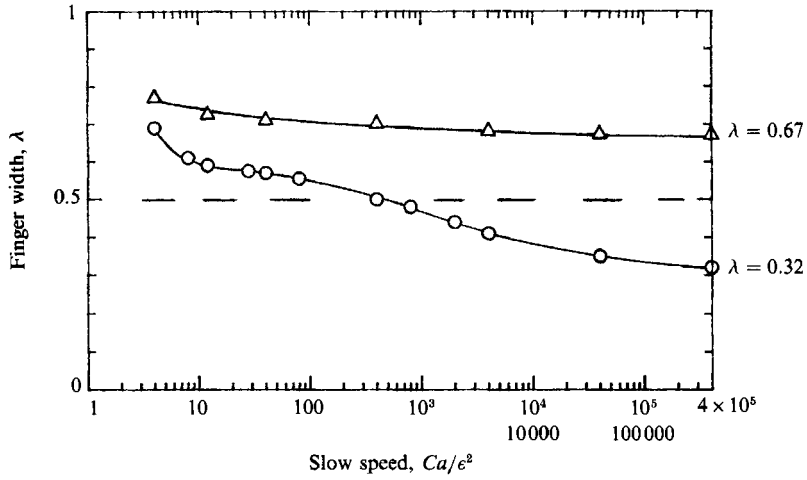

FIGURE 11. The dependence of the finger width on the slow speed variable, C_2: △, $\gamma/C_2 = 0.5$ and $\Theta_R = 90°$. ○, $\gamma/C_2 = 0.05$ and $\Theta_R = 90°$.

γ	λ_0	λ_1	λ_2
0	0.55	0.68	0.84
2	0.57	0.70	0.85
10	0.65	0.77	0.90
20	0.71	0.83	—

TABLE 1. Solutions to the C_2 problem

of viscous fingers observed by Kopf-Sill & Homsy, and the characteristics predicted by our analysis of viscous fingers possessing moving contact lines.

We begin by examining the characteristics of the C_2 problem, since this corresponds most closely to the thin film viscous fingering problem which has been studied extensively by others. When γ equals zero and Θ_R equals $\frac{1}{2}\pi$, the equations describing the shape of the finger are identical for both problems. Our results $\{\lambda_i \mid \gamma = 0, i = 0, 1, 2\}$ agree with the finger widths corresponding to the three cases reported by Vanden-Broeck (1983) at $K = 0.273$. (Our K corresponds to Vanden-Broeck's K. Also, the agreement is to the two significant figures which he reports.) Our principal conjecture for the C_2 problem is that the physically relevant solution for positive values of γ corresponds to the finger with the smallest width, λ_0. This has been shown to be the case when γ equals zero, through favourable comparisons between experiment and theory and by stability considerations, as discussed in §1. The basis for this speculation of stability for values of γ other than zero is that solutions for small values of γ differ only by small amounts from the solution for γ equal to zero, i.e. the problem does not appear to be singular at γ equals zero. Figure 9 illustrates by way of an example the continuity of $\{\lambda_i \mid i = 0, 1, 2\}$ at γ equals zero; also refer to table 1. Further supporting evidence lies in the similarity of the shapes of the fingers near the nose. For the case of λ_0, they are all well-rounded, regardless of the value of γ (refer to figure 10*a*). Likewise, all the other solutions, i.e. $\{\lambda_i \mid i = 1, 2\}$, are either broad and flat, or undulate (refer to figures 10*b* and *c*). Thus, if the solutions corresponding to $\{\lambda_i \mid i = 1, 2\}$ are not physically relevant for γ equals zero, it seems plausible that they are all not physically relevant for values of γ greater than zero.

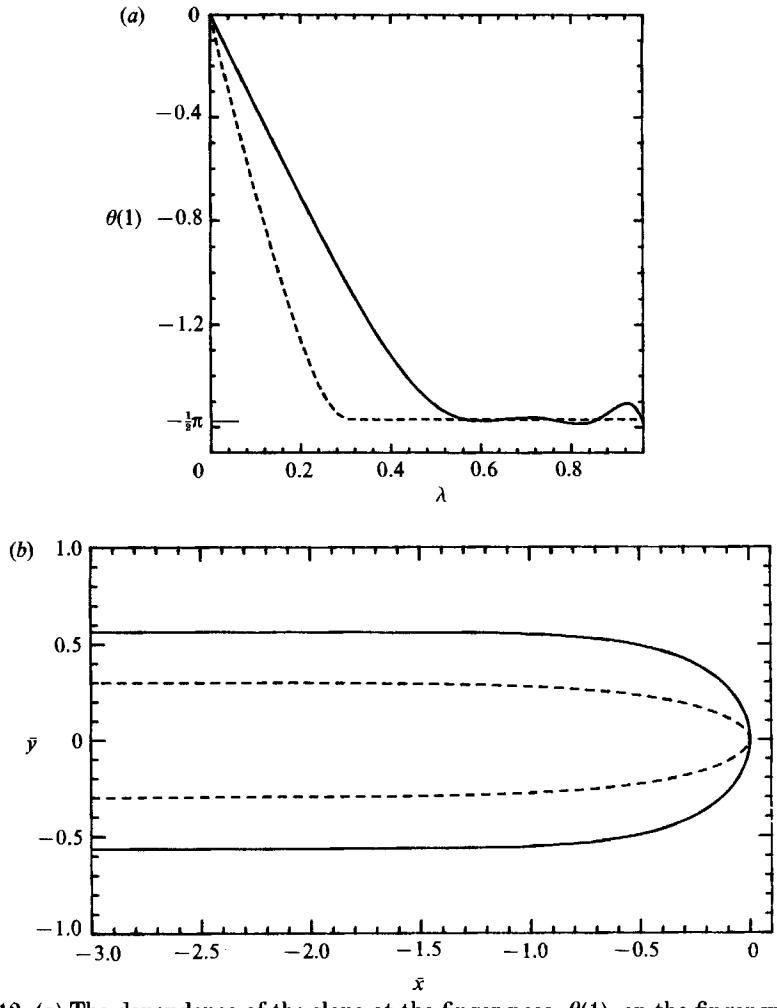

FIGURE 12. (*a*) The dependence of the slope at the finger nose, $\theta(1)$, on the finger width, λ, and (*b*) finger shapes corresponding to λ_0 values from (*a*) for $\gamma/C_2 = 0.05$ and $\Theta_R = 90°$. ——, $C_2 = 80$, $\lambda_0 = 0.57$; - - - - -, $C_2 = 4 \times 10^6$, $\lambda_0 = 0.30$.

The complete results for two examples are given in figure 11. Note that the finger widths in the limit as $C_2 \to \infty$ depend on the values of $(\epsilon\sigma/\mu)\,\mathrm{d}\theta/\mathrm{d}U$ and Θ_R. They are not approximately equal to 0.5, as in the case when thin films are present.

We identify the physically relevant solution to the C_1 problem by establishing the following relationship between the C_1 and C_2 problems: the limit as $C_2 \to \infty$, holding $(\epsilon\sigma/\mu)\,\mathrm{d}\theta/\mathrm{d}U$ and Θ_R fixed, is equivalent to the limit as $C_1 \to 0$, holding $(\epsilon\sigma/\mu)\,\mathrm{d}\theta/\mathrm{d}U$ and Θ_R fixed.† Evidence demonstrating the validity of this relationship consists of calculating identical slopes at the nose of the finger for $\lambda \in [0, 0.96]$ for the C_1 and C_2 problems (for a particular example, refer to figures 12*a* and 5*a*), and obtaining identical finger shapes corresponding to λ_0 and λ_m (refer to figures 12*b* and 5*b*). Thus, if λ_0 is the physically relevant solution to the C_2 problem, then it seems plausible that

† This equivalence breaks down for $(\epsilon\sigma/\mu)\,\mathrm{d}\theta/\mathrm{d}U \equiv 0$, or $\theta_R \equiv 0$, because each implies that $\beta = 0$. When $\beta = 0$, the C_2 problem is equivalent to the thin film viscous fingering problem posed by McLean & Saffman, and the C_1 problem is equivalent to the problem posed by Saffman & Taylor. It is now well known that the problem posed by McLean & Saffman is singular as $C_2 \to \infty$.

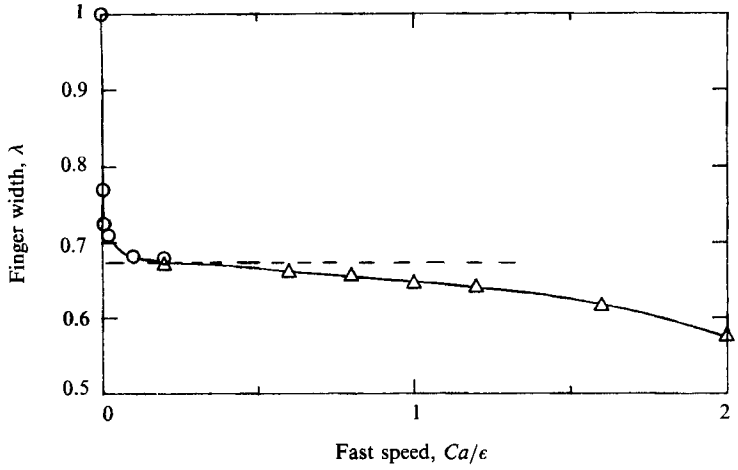

FIGURE 13. The dependence of the finger width on the fast speed variable, C_1, for $\beta/C_1 = 0.5$, $\epsilon = 5 \times 10^{-4}$, and $\Theta_R = 90°$. △, Results of C_1 problem; ○, results of C_2 problem.

λ_m is the physically relevant solution for the C_1 problem. We conjecture that λ_m represents the physically relevant solution to the C_1 problem for values of C_1 other than zero. A composite plot of the results of the C_1 and C_2 problems for a particular example is illustrated in figure 13. Thus, it is natural to refer to C_2 as the 'slow' finger speed solution and C_1 as the 'fast' finger speed solution, at least slow and fast relative to each other. Note the similarity in appearance between our figure 13 and figure 8 in Reinelt (1987*b*). We are not suggesting that thin film problems can be viewed as moving contact line problems, in light of the remarks made at the beginning of § 1, but rather that retaining only the gapwise component of the jump in pressure at the fluid interface caused by the variation in thickness of the deposited film along the finger may be sufficient at large values of C_2; thus, the affect of the jump in pressure due to the spanwise change in curvature on the finger width or the finger shape may not be significant. The similarity between these two figures also suggests that the thin film problem may be described by multiple velocity scales.

It is of interest to note that the width of the finger appears to be sensitive to the dynamics of the fluid at its nose. This is evident when the influence of Θ_R is examined. When $\beta = \Theta_R$, the contact angle at the nose is always zero, regardless of the value of Θ_R. Figure 7 indicates that λ_m is relatively insensitive to Θ_R. On the other hand, when $\beta = 0$, the contact angle at the nose is Θ_R. For this case, figure 7 indicates that λ_m is sensitive to Θ_R. This is reminiscent of experimental observations of the dynamics of viscous fingers with thin films. The width of these fingers have been shown to be sensitive to the presence of rather small bubbles or wires positioned at its nose (Couder, Gérard & Rabaud 1986).

Finally, we point out some similarities between the behaviour of viscous fingers with moving contact lines, and the experimental observations of Kopf-Sill & Homsy. Kopf-Sill & Homsy performed experiments of air displacing glycerine through a glass Hele-Shaw cell for different size gaps. They find what the refer to as a new class of solutions to the shape selection problem, characterized by rather narrow fingers in the limit of large values of C_2 (the finger widths can take on values much less than 0.5), whose finger widths vary directly with the aspect ratio of the cell, ϵ. It is interesting to note that this behaviour also characterizes our C_2 problem, as has already been discussed in the example illustrated in figure 11.

REFERENCES

BENSIMON, D. 1986 Stability of viscous fingering. *Phys. Rev.* A **33**, 1302.

BRETHERTON, F. P. 1961 The motion of long bubbles in tubes. *J. Fluid Mech.* **10**, 166.

COUDER, Y., GÉRARD, N. & RABAUD, M. 1986 Narrow fingers in the Saffman–Taylor instability. *Phys. Rev.* A **34**, 5175.

DUSSAN, V. E. B. 1979 On the spreading of liquids on solid surfaces: static and dynamic contact lines. *Ann. Rev. Fluid Mech.* **11**, 371.

KESSLER, D. A. & LEVINE, H. 1985 Stability patterns in Hele-Shaw cells. *Phys. Rev.* A **32**, 1930.

KOPF-SILL, A. R. & HOMSY, G. M. 1987 Narrow fingers in a Hele-Shaw cell. *Phys. Fluids* **31**, 2607.

KOPF-SILL, A. R. & HOMSY, G. M. 1988 Bubble motion in a Hele-Shaw cell. *Phys. Fluids* **31**, 18.

MCLEAN, J. W. & SAFFMAN, P. G. 1981 The effect of surface tension on the shape of fingers in a Hele-Shaw cell. *J. Fluid Mech.* **102**, 455.

NGAN, C. G. & DUSSAN, V. E. B 1989 On the dynamics of liquid spreading on solid surfaces. *J. Fluid Mech.* **209**, 191.

PARK, C. W. & HOMSY, G. M. 1984 Two-phase displacement in Hele-Shaw cells: theory. *J. Fluid Mech.* **139**, 291.

REINELT, D. A. 1987*a* Interface conditions for two-phase displacement in Hele-Shaw cells. *J. Fluid Mech.* **183**, 219.

REINELT, D. A. 1987*b* The effect of thin film variations and transverse curvature on the shape of fingers in a Hele-Shaw cell. *Phys. Fluids* **30**, 2617.

REINELT, D. A. & SAFFMAN, P. G. 1985 The penetration of a finger into a viscous fluid in a channel and tube. *SIAM J. Sci. Stat. Comput.* **6** (3), 542.

ROMERO, I. A. 1981 The fingering problem in a Hele-Shaw cell. PhD thesis, California Institute of Technology.

SAFFMAN, P. G. & TANVEER, S. 1989 Prediction of bubble velocity in a Hele-Shaw cell: Thin film and contact angle effects. *Phys. Fluids* A **1** (2), 219.

SAFFMAN, P. G. & TAYLOR, G. I. 1958 The penetration of a fluid into a porous medium of Hele-Shaw cell containing a more viscous liquid. *Proc. R. Soc. Lond.* A **245**, 312.

SCHWARTZ, L. W. & DEGREGORIA, A. J. 1987 Simulation of Hele-Shaw fingering with finite-capillary-number effects included. *Phys. Rev.* A **35**, 276.

TABELING, P. & LIBCHABER, A. 1986 Film draining and the Saffman–Taylor Problem. *Phys. Rev.* A **33**, 794.

TABELING, P., ZOCCHI, G. & LIBCHABER, A. 1987 An experimental study of the Saffman–Taylor instability. *J. Fluid Mech.* **177**, 67.

TANVEER, S. & SAFFMAN, P. G. 1987 Stability of bubbles in a Hele-Shaw cell. *Phys. Fluids* **30**, 2624.

VANDEN-BROECK, J. M. 1983 Fingers in a Hele-Shaw cell with surface tension. *Phys. Fluids* **26**, 2033.

WEINSTEIN, S. J. 1988 A theoretical study of two-phase Hele-Shaw flow with a moving contact line. PhD thesis, University of Pennsylvania.